Schweizerischer Erdbebendienst
Service Sismologique Suisse
Servizio Sismico Svizzero
Swiss Seismological Service

ETH zürich

SITE CHARACTERIZATION REPORT

SHEK: Heerbrugg (SG) - Kantonsschule

Manuel Hobiger, Paolo Bergamo, Clotaire Michel, Donat Fäh

Last Modification: 23rd February, 2017

Schweizerischer Erdbebendienst (SED)
Service Sismologique Suisse
Servizio Sismico Svizzero
Servizi da Terratrembels Svizzer

ETH Zürich
Sonneggstrasse 5
8092 Zürich
Schweiz
manuel.hobiger@sed.ethz.ch

Contents

1 Summary

The free-field strong-motion station SHEK was built next to the Kantonsschule in Heerbrugg (SG). It replaces the old station SMTK in Montlingen, about 10 km south of Heerbrugg. We performed two passive seismic arrays with different size for the site characterization. The site characterization measurements showed that the fundamental frequency of the structure beneath the station is about 1.6 Hz. The polarization analysis also showed a two-dimensional polarization of the valley at this frequency, but the frequency of the ellipticity peak also changes in the larger array and we inverted the measurements assuming a 1-dimensional structure.
The array measurements were analyzed with three different techniques, namely 3-component HRFK, WaveDec and SPAC. All techniques gave similar dispersion curves. The fundamental mode Love and Rayleigh wave dispersion curves could be retrieved at both arrays, but there are minor discrepancies between the results of both array. Joint inversions of dispersion and ellipticity curves yielded a superficial layer of around 9 m thickness with a shear-wave velocity of about 150 m/s, followed by a second layer of less than 280 m/s down to about 50 m, where the seismic bedrock of subalpine molasse is found. The V_{S30} value is around 220 m/s (ground type C in EC8 and D in SIA261).

2 Introduction

In the framework of the second phase of the Swiss Strong Motion Network (SSMNet) renewal project, a new station was planned in the Rhine Valley in the canton St. Gallen. The site was planned as renewal of the old strong motion station SMTK in Montlingen, 10 km south of Heerbrugg. SMTK could not be replaced at the same site. The site selection resulted in the Kantonsschule in Heerbrugg being the best site from the risk and noise aspects. The new station, called SHEK, was constructed in the western part of the school area and went operational on 17 November 2015. The location of the station is shown in Fig. 1.

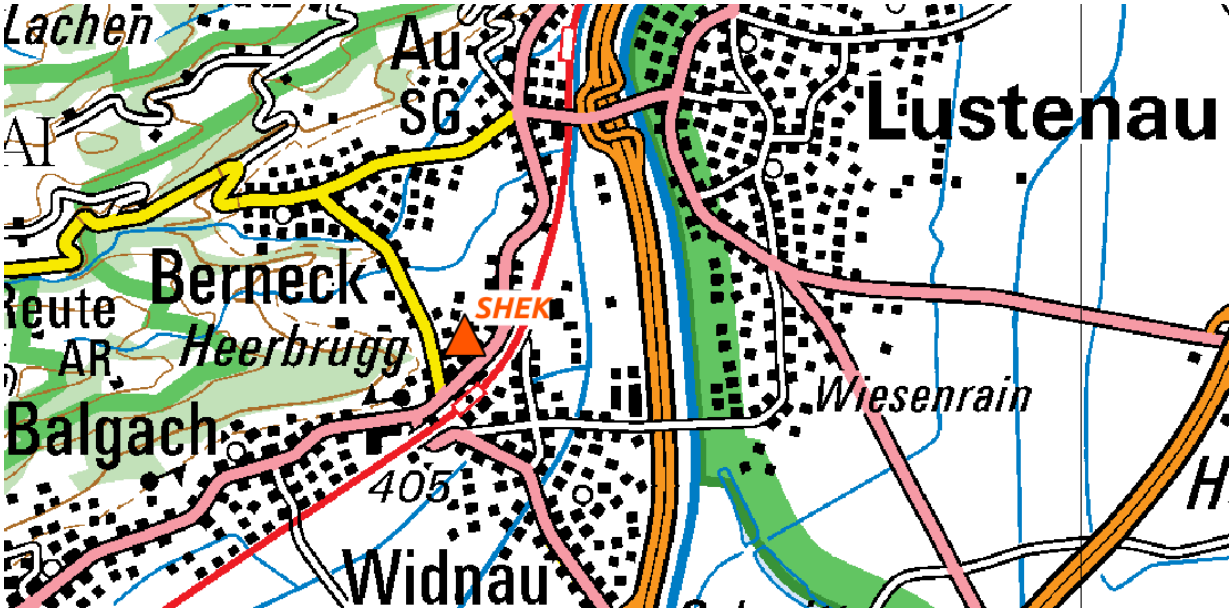

Figure 1: Map showing the location of station SHEK in Heerbrugg.

3 Geological setting

A geological map of the surroundings of station SHEK is shown in Fig. 2. The station is located inside the deep Rhine Basin. A nearby borehole (blue circle in the map) found the subalpine molasse at a depth of 30 m.

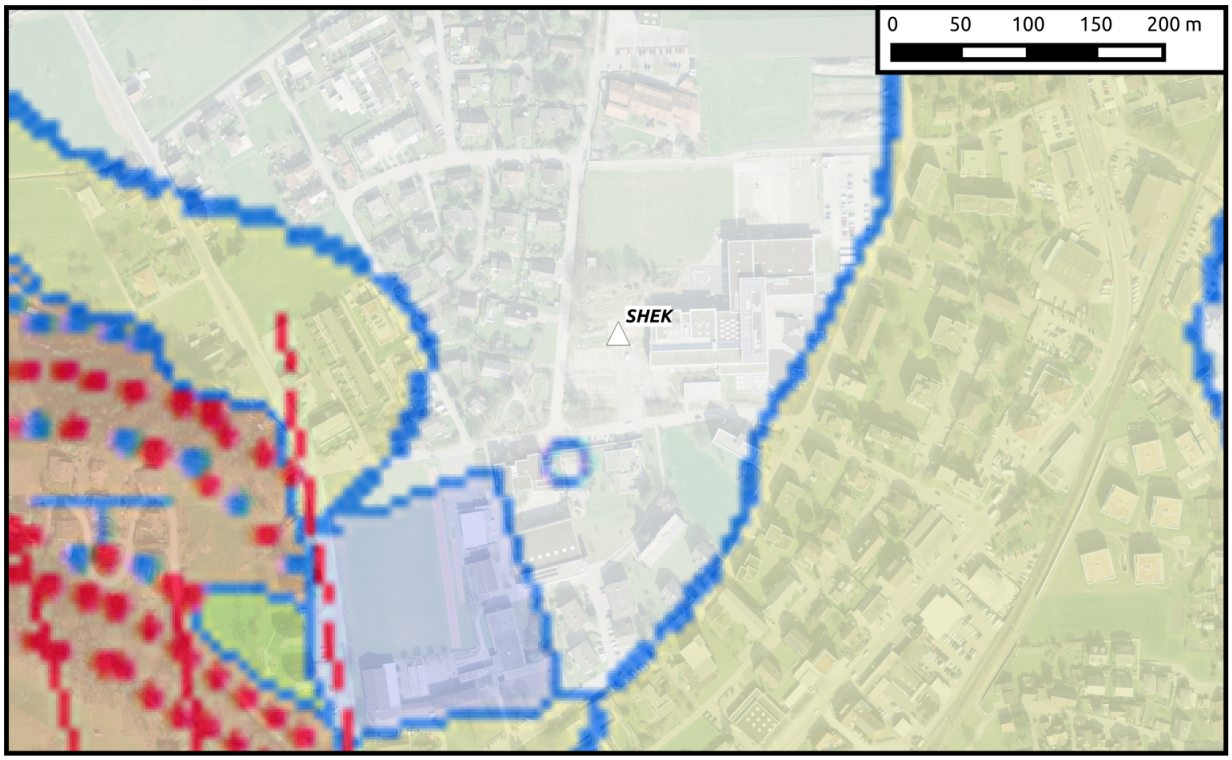

Figure 2: Geological map of the area around station SHEK. According to the geological atlas, station SHEK lies on young quarternary alluvia (light gray). The yellow ochre area corresponds to postglacial quaternary alluvia, the light blue area to artificial underground and the brown area in the southwest to subalpine molasse.

4 Site characterization

4.1 Measurements and data set

In order to characterize the local underground structure around station SHEK, passive seismic array measurements were carried out on 2016 July 19. The layout of the two seismic arrays is shown in Fig. 3.
Array 1 was installed first, it consisted of 16 stations in total. It was planned as consisting of a central station and three rings of five stations each with radii of 8, 20 and 50 m. The station names of this first array are composed of "SHEK" followed by a two-digit number between 42 and 72.
In order to measure longer wavelengths and reach deeper layers, a second array was built with 12 stations. The layout of the second array consists of two rings of five stations. Stations SHEK43 and SHEK48 of the first array were also used for the second array, the other stations of the second array have names consisting of "SHEK" followed by a two-digit number between 82 and 95.
The parameters of both arrays are given in Table 1.
The station locations have been measured by a differential GPS system (Leica Viva GS10) which was set up to measure with a precision better than 5 cm. All station locations were measured with better precisions than this. Only station SHEK93 had a precision of 5.3 cm.

Table 1: List of the seismic array measurements in Heerbrugg.

Array name	Number of sensors	Minimum interstation distance [m]	Maximum interstation distance [m]	Recording time [s]
1	16	8.0	98.9	6600
2	12	44.9	586.7	7200

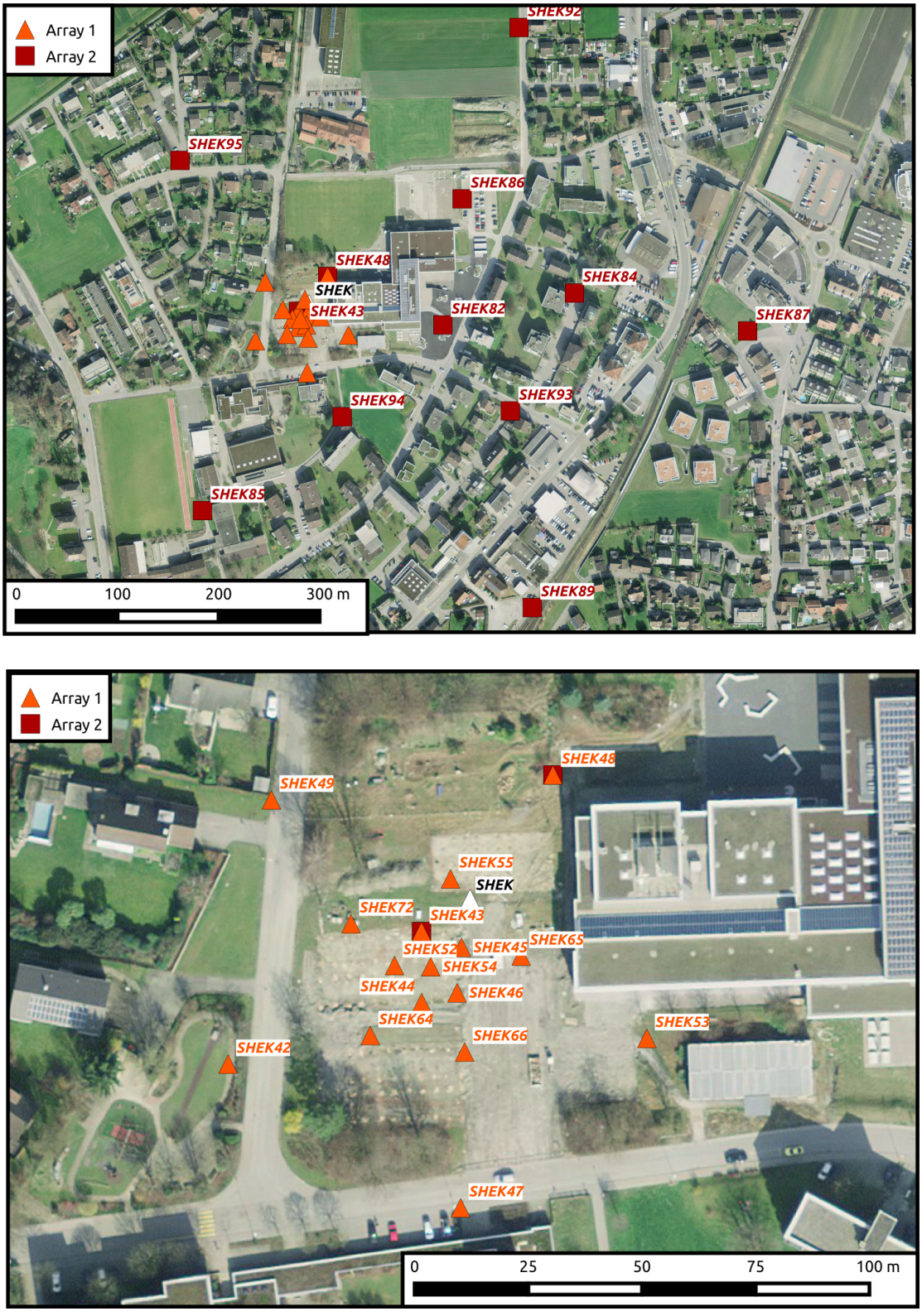

Figure 3: Layout of the array measurements around station SHEK. The location of SHEK is indicated by the white triangle, the locations of the stations during the first array measurement by orange triangles and during the second array measurement by red squares. ©2017 swisstopo (JD100042)

4.2 Measurement results

4.2.1 H/V curves

Figure 4 shows the H/V curves determined with the time-frequency analysis method (Fäh et al., 2009) for all stations of both arrays. In the small array, the curves for the different stations look extremely similar. The one station which has a slightly different peak is station SHEK49. All stations have peak frequencies of around 1.6 Hz.
For the large array, the curves are more scattered and the peak frequencies range from 0.7 to 2.0 Hz. Fig. 5 shows a map of the peak frequencies at the different stations. Peak frequencies below 1 Hz are observed for stations SHEK84, SHEK87, SHEK89 and SHEK92, which are in the eastern part and lie over deeper sediments. The highest peak frequency (2.0 Hz) belongs to station SHEK85, which is the westernmost station over the shallowest sediments.

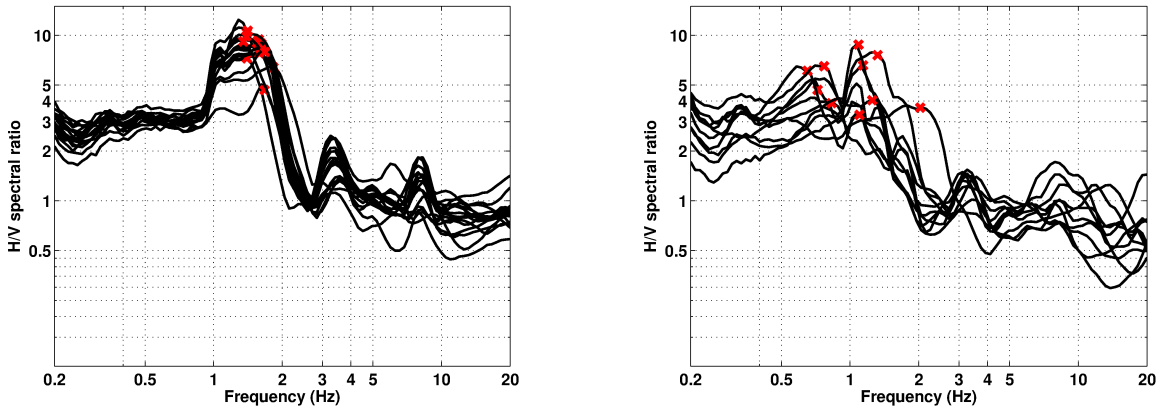

Figure 4: Overview of the H/V measurements for the different stations of first (left) and the second (right) array measurement.

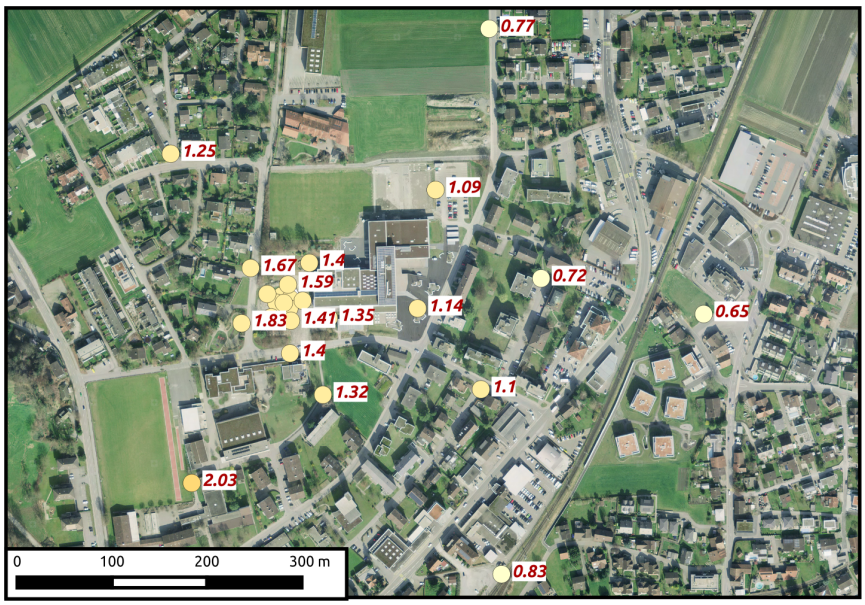

Figure 5: Overview of the H/V frequency peaks at the different stations. ©2017 swisstopo (JD100042)

4.2.2 RayDec ellipticity curves

The RayDec technique (Hobiger et al., 2009) is meant to eliminate the contributions of other wave types than Rayleigh waves and give a better estimate of the ellipticity than the classical H/V technique. The RayDec ellipticity curves for all stations of the array measurements are shown in Fig. 6.
In the small array, the RayDec curves are similar to the H/V curves. All stations show a peak around 1.6 Hz and the peaks are quite broad between 1 and 2 Hz. Secondary peaks can be seen around 3 and 8 Hz. In the large array, the RayDec curves are very erratic with a lot of scattering between the different stations.

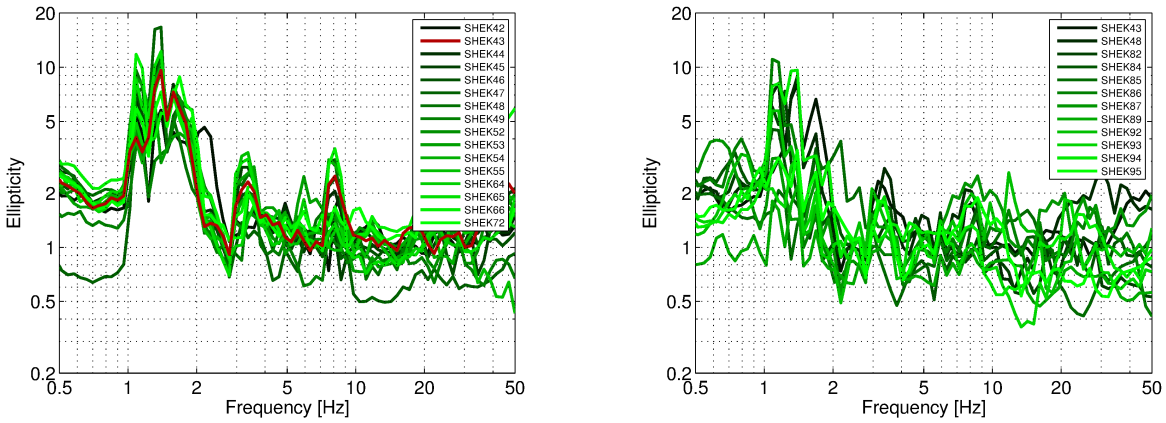

Figure 6: RayDec ellipticities for array 1 (left) and array 2 (right).

4.2.3 Polarization measurements

The polarization parameters of the seismic noise recordings of all stations of the two arrays are similar. Only the results for SHEK43 are shown here. The analysis was performed according to Burjánek et al. (2010) and Burjánek et al. (2012).
The particle motion is linearly polarized between 1 and 2 Hz, i.e. at the fundamental frequency of the array. The polarization in this frequency is mostly north-south, which matches mostly with the valley direction. However, the Rhine Valley at this location is oriented in a more northeasterly direction (about 30°E), but the location of our measurements is also close to the western edge of the valley, so that local effects from the vicinity of the border cannot be excluded. Nevertheless, this behavior seems to indicate 2-dimensional wave propagation effects in the valley.

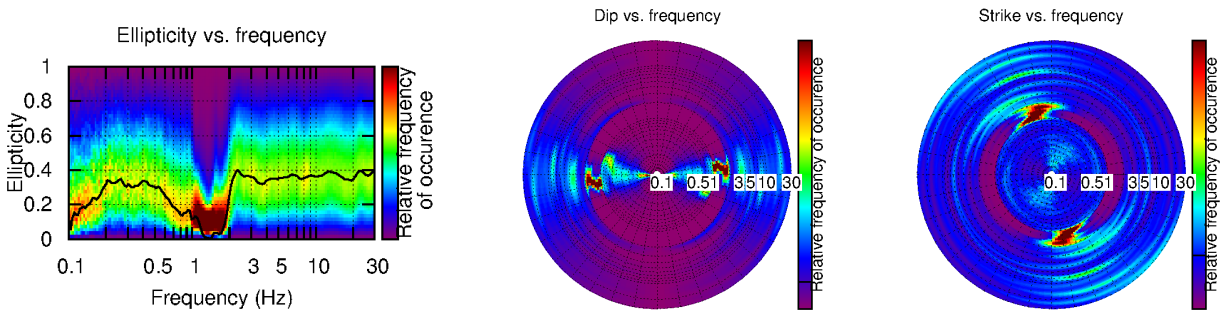

Figure 7: Polarization analysis of station SHEK43.

4.2.4 3-component high-resolution FK

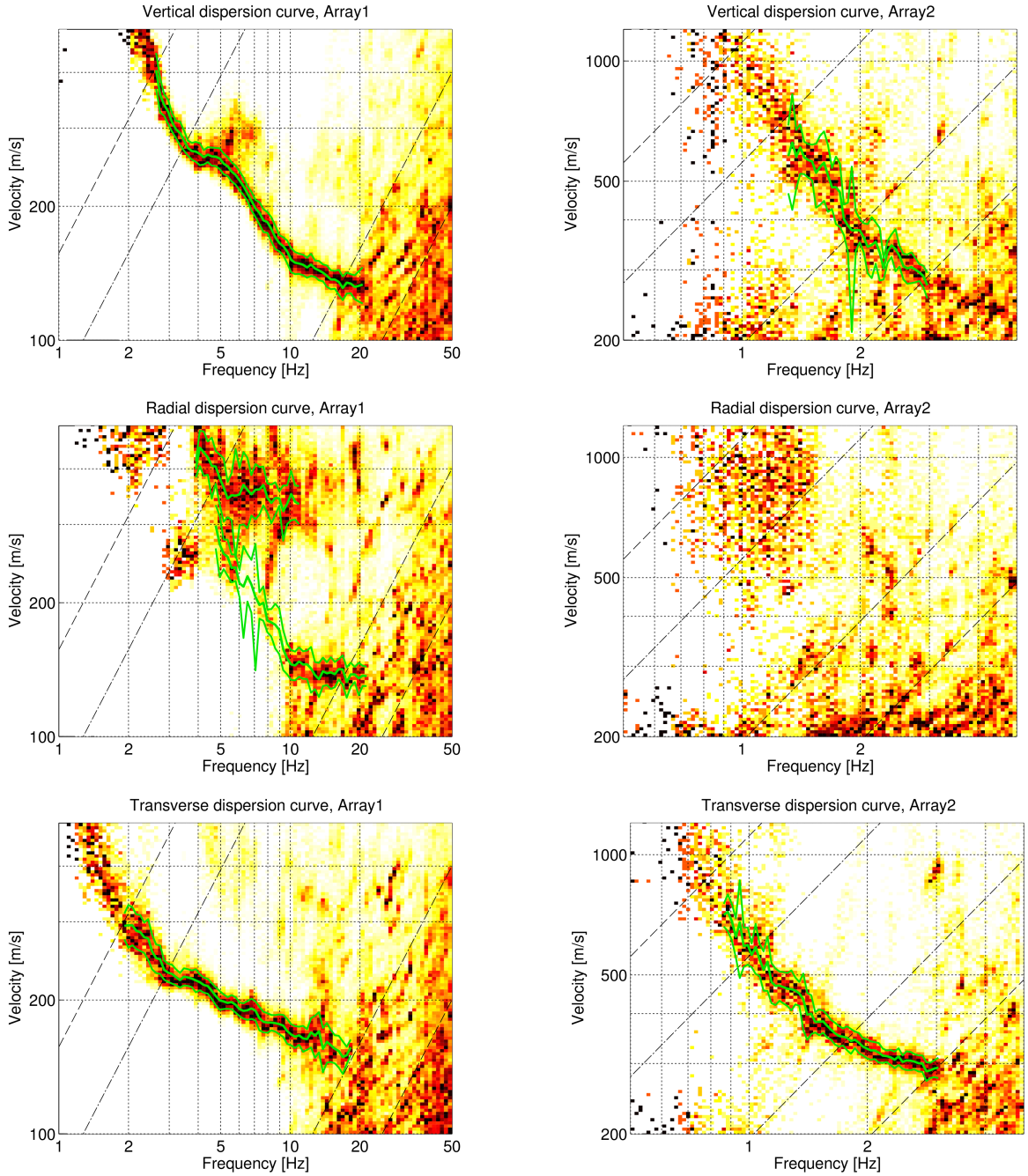

Figure 8: Dispersion curves obtained with the 3-component HRFK algorithm (Poggi and Fäh, 2010). In the left column, the results for array 1 are shown, in the right column for array 2. From top to bottom the results for the vertical, radial and transverse components are shown. The dashed and dotted black lines are the array resolution limits. The solid green lines are picked from the data, where the central line indicates the best values and the two outer lines the standard deviation.

The results of the 3-component high-resolution FK analysis (Poggi and Fäh, 2010) of both arrays are shown in Figs 8 and 9. On the vertical component, the fundamental mode of the Rayleigh waves is clearly visible in array 1 between 3 and 20 Hz. In array 2, the result is less clear, but the curve can be retrieved down to about 1.4 Hz without reaching the lower resolution limit. On the radial component, the results are less clear in array 1, where two modes can be picked. In array 2, no dispersion curve can be identified. The transverse dispersion curves can be well retrieved in both arrays and seem to fit together quite well.
The ellipticity curves determined with the 3-component HRFK analysis are shown in Fig. 9.

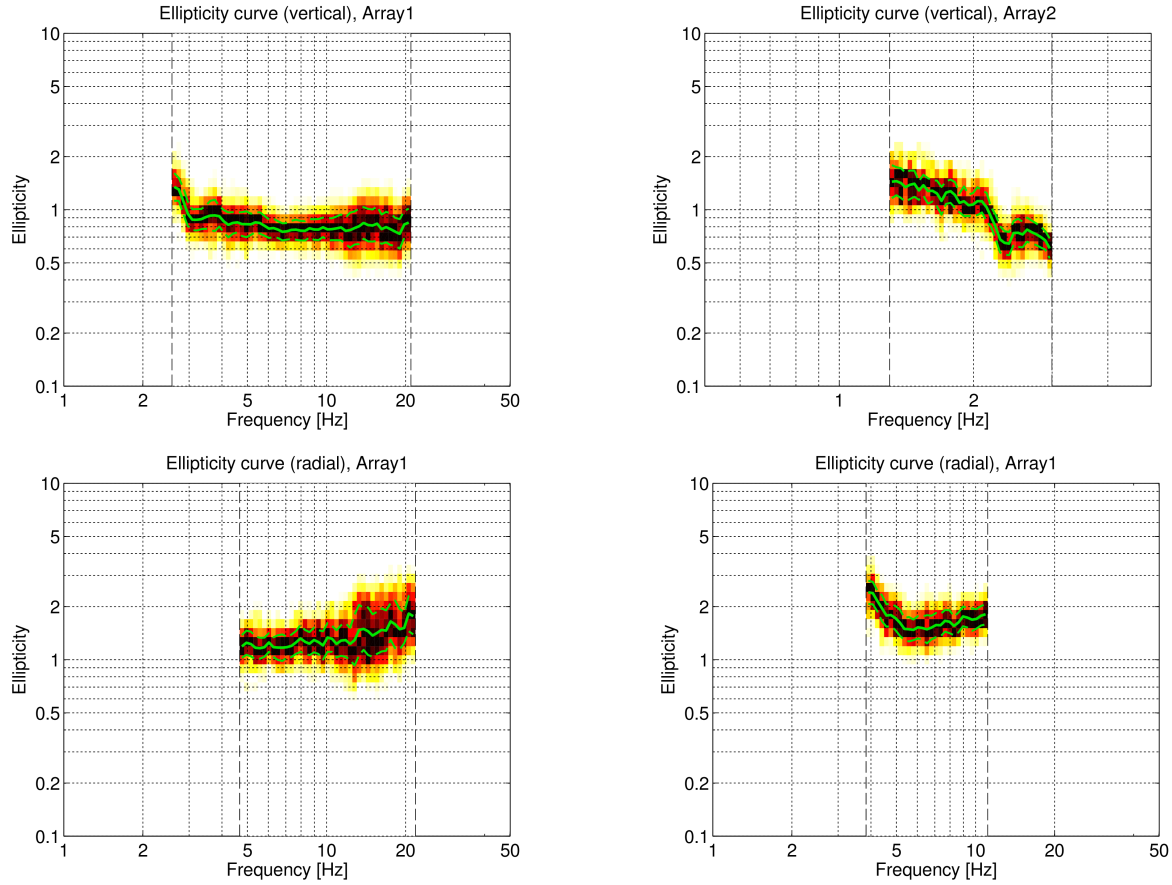

Figure 9: Ellipticity curves obtained with the 3-component HRFK algorithm (Poggi and Fäh, 2010) for the vertical component picked in array 1 (top, left) and array 2 (top, right) and for the radial component for the first mode (bottom, left) and the second mode (bottom, right) picked in array 1. The frequency ranges of the different curves correspond to the ranges where the dispersion curves had been picked.

4.2.5 WaveDec

The results of the WaveDec (Maranò et al., 2012) processing are shown in Fig. 10. This technique estimates the properties of single or multiple waves simultaneously with a maximum likelihood approach. In order to get good results, the parameter γ, which modifies the sharpness of the wave property estimation, has been tuned. The best results are obtained with $\gamma = 0.3$. Anyhow, the resulting curves are less clearly retrieved than with the 3-C HRFK.
In array 1, the Love wave dispersion curve can be retrieved between 2 and 12 Hz, but with a lot of scattering. In array 2, the resolution is better, but the lower resolution limit cannot be reached. The curve here can be picked between about 1 and 3 Hz.
The Rayleigh wave dispersion curve can be obtained in array 1 from about 4 to 23 Hz, again not reaching the lower resolution limit of the array. For array 2, no reliable dispersion curve could be picked at all. The ellipticity angle for the picked dispersion curve indicates prograde particle motion below 2.8 Hz and retrograde particle motion above, corresponding to a singular trough at 2.8 Hz. At higher frequencies, the ellipticity angle is mostly flat, with values around -20°, i.e. ellipticities of about 0.4.

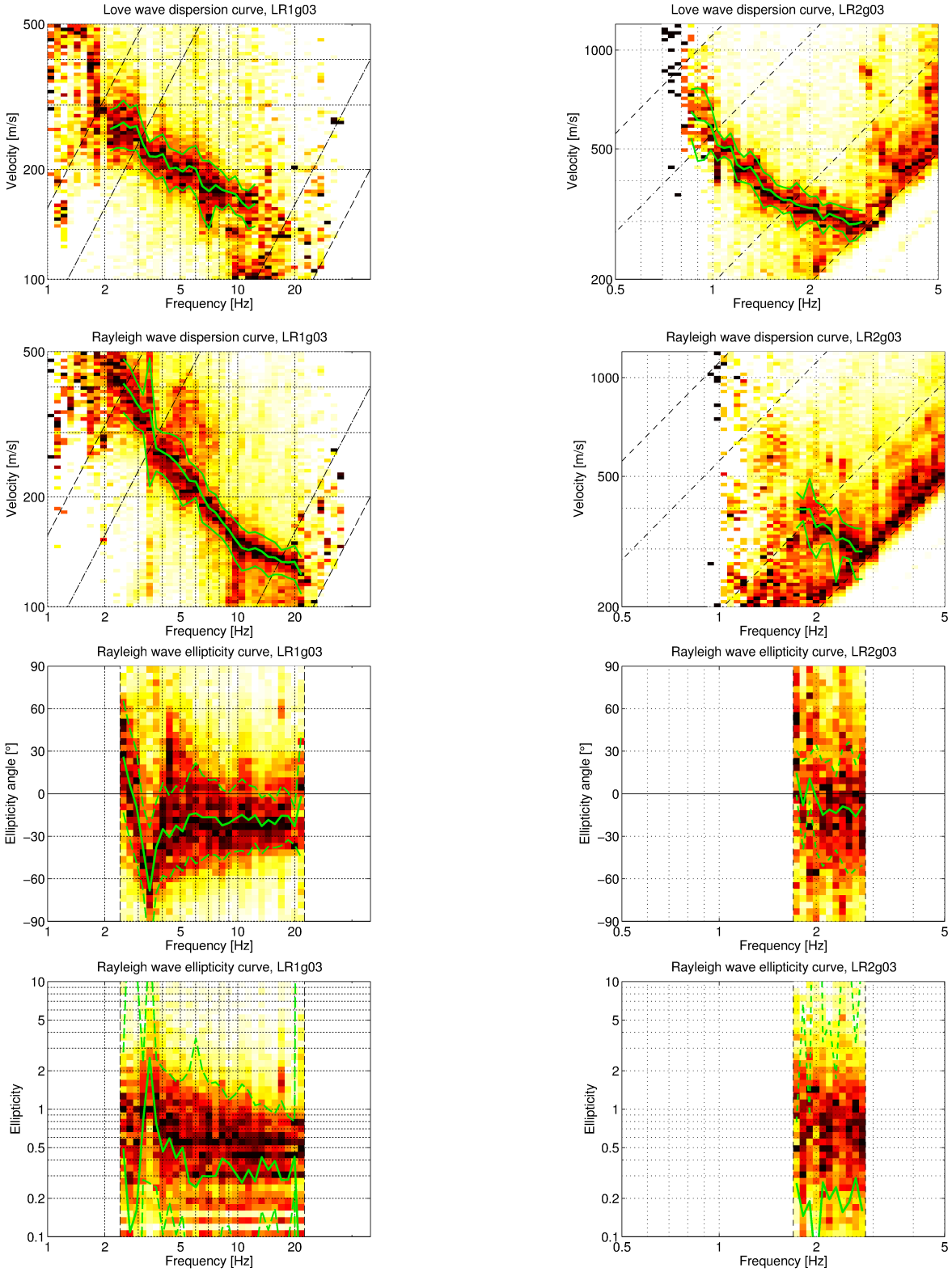

Figure 10: Love and Rayleigh wave dispersion and ellipticity curves obtained with the WaveDec technique (Maranò et al., 2012). The dashed lines indicate the theoretical array resolution limits. From top to bottom: Love wave dispersion curve, Rayleigh wave dispersion curve, Rayleigh wave ellipticity curve represented as ellipticity angle, Rayleigh wave ellipticity, i.e. the absolute value of the tangent of the ellipticity angle, all for array 1 (left) and array 2 (right).

4.2.6 SPAC

The SPAC (Aki, 1957) curves of the vertical components have been calculated using the M-SPAC (Bettig et al., 2001) technique implemented in geopsy. Rings with different radius ranges had been defined previously and for all station pairs with distance inside this radius range, the cross-correlation was calculated in different frequency ranges. These cross-correlation curves are averaged for all station pairs of the respective ring and give the SPAC curve. The rings are defined in such a way that at least three station pairs contribute and that their connecting vectors have a good directional coverage.
The SPAC curves for all defined rings are shown in Figs 11-12, respectively. The black points indicate the data values which contributed to the final dispersion curve estimation, which was made with the function `spac2disp` of the geopsy package. These resulting dispersion curves are shown in Fig. 13.
For array 1, whose array layout was optimized for SPAC, there were a multitude of rings with different distance ranges which give results very close to the theoretically expected Bessel functions. The dispersion curve can be retrieved between 2 and 12 Hz. For array 2, there are less rings with worse quality, but the dispersion curve can nevertheless be determined between 0.6 and 3 Hz.

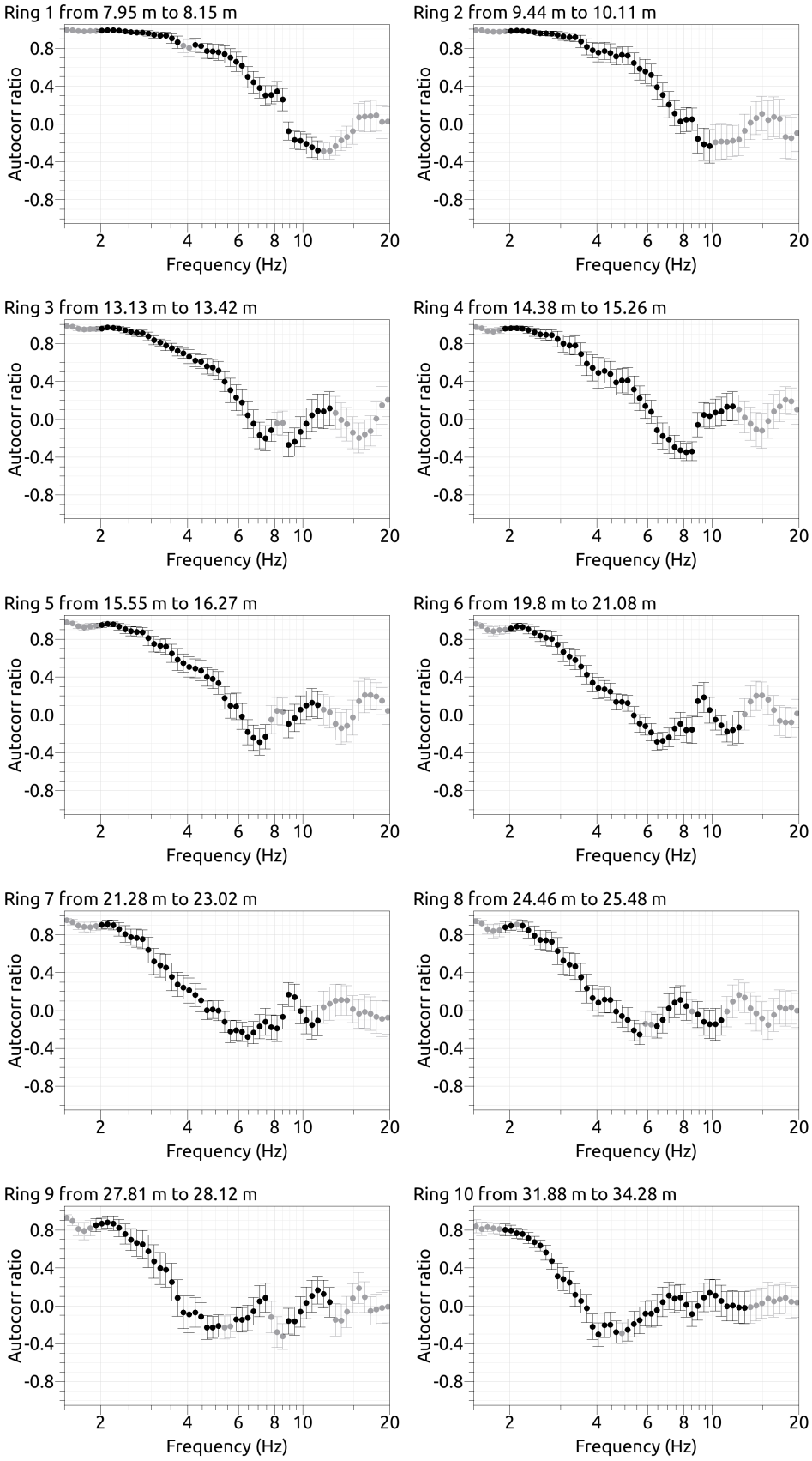

Figure 11: SPAC curves for array 1. The black data points contributed to the dispersion curve estimation.

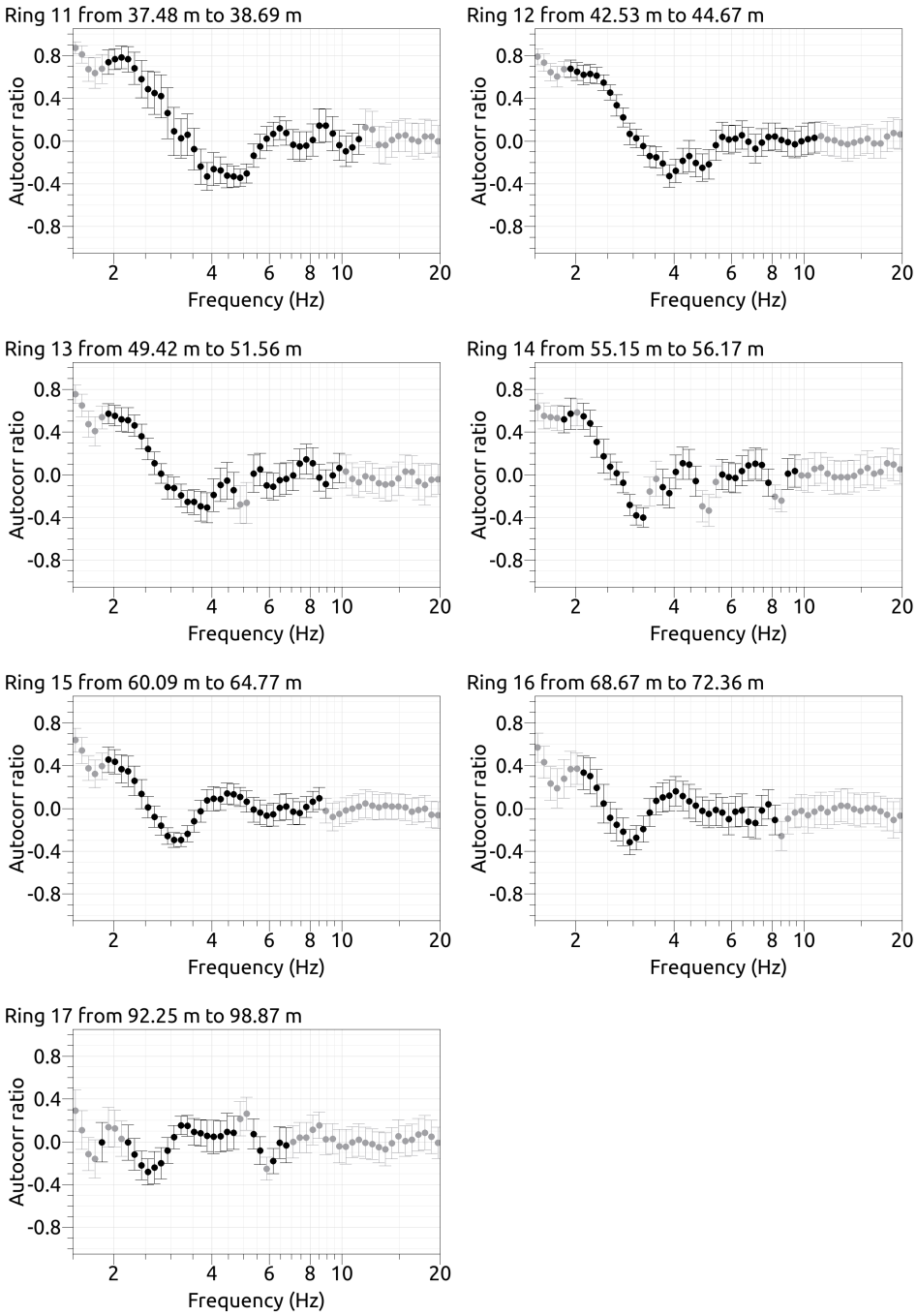

Figure 11: continued.

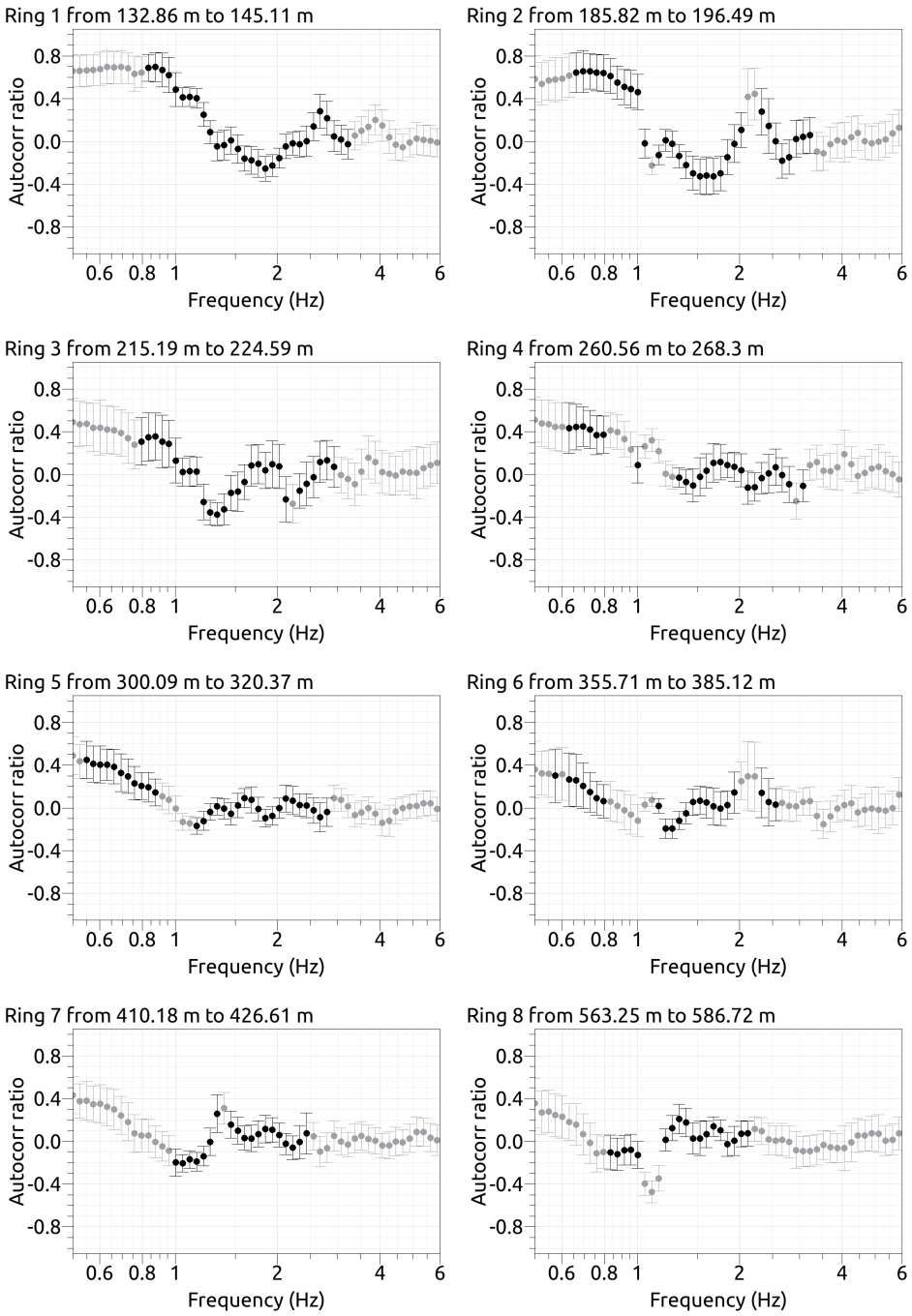

Figure 12: SPAC curves for array 2. The black data points contributed to the dispersion curve estimation.

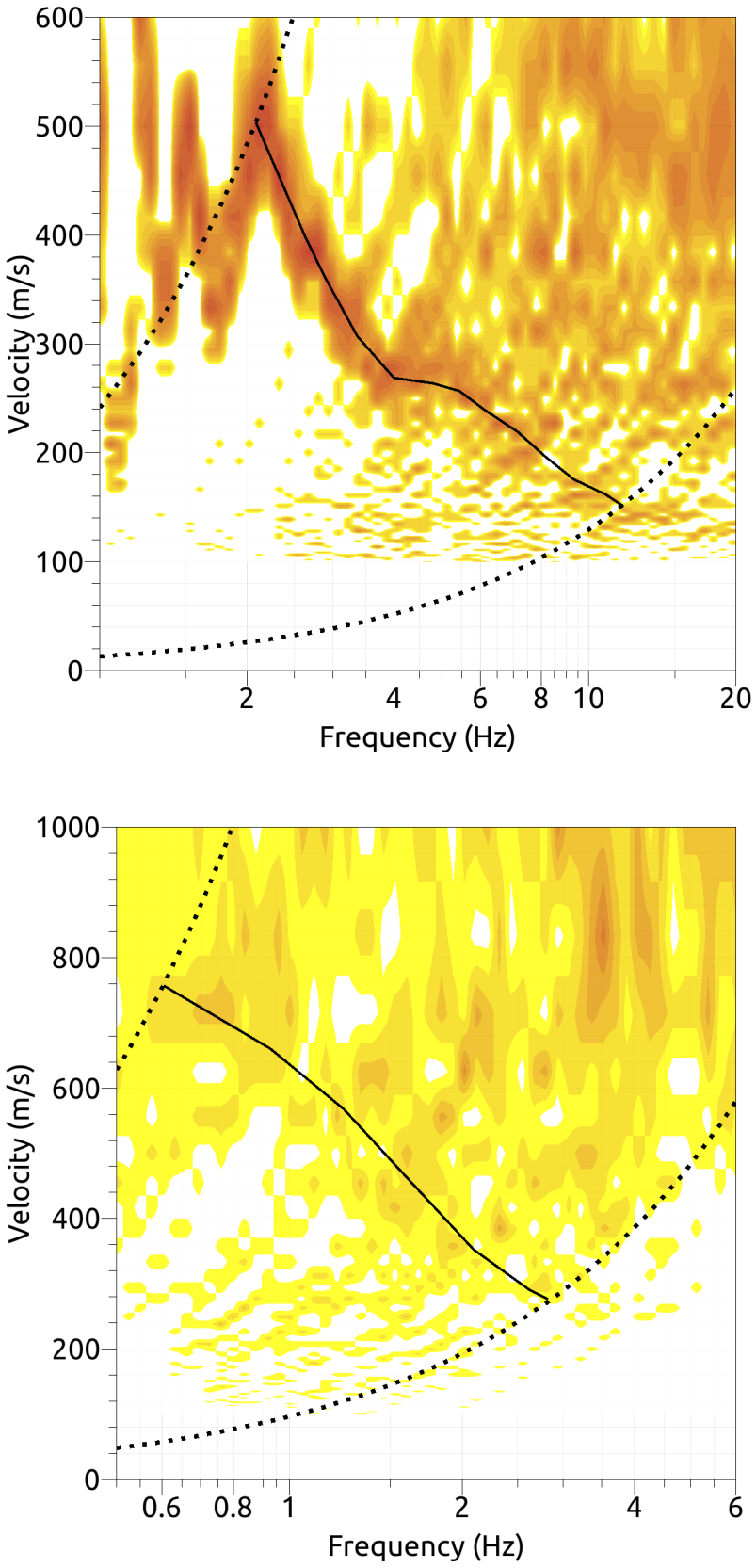

Figure 13: Resulting Rayleigh wave velocities for array 1 (top) and array2 (bottom). The black line corresponds to the picked dispersion curve. The black curves are resolution limits, which are different from the FK analysis resolution limits.

4.3 Summary

Fig. 14 gives an overview of the dispersion and ellipticity curves determined by the different methods.
For Love waves, the HRFK and WaveDec results for the respective arrays are in good agreement, but there is a gap between the results of both arrays between 2 and 3 Hz.
For the Rayleigh waves, there is also general agreement between the different methods, but a discrepancy between both arrays. For array 1, the curves from HRFK (vertical and radial), WaveDec and SPAC agree substantially. For array 2, HRFK and SPAC retrieve the Rayleigh wave dispersion curve for a broader frequency range than WaveDec. The discrepancy between both arrays between 2 and 3 Hz is here the opposite of the Love waves, as the smaller array shows higher velocities than the large one for the Rayleigh waves.
There are large differences between the ellipticity curves of the different methods, but the interesting part of the curve around the fundamental peak is outside of the resolution limits of both arrays. The ellipticity trough found with WaveDec in the small array is in good agreement with the supposed trough from the RayDec ellipticity.
The polarization measurements indicated a 2-dimensional site effect exactly at the frequency range of the ellipticity peak. However, the ellipticity peaks differ from site to site in the large array, which should not be the case if the valley reacted as a whole. Therefore, we assume that the structure is 1-dimensional and invert for such a structure.

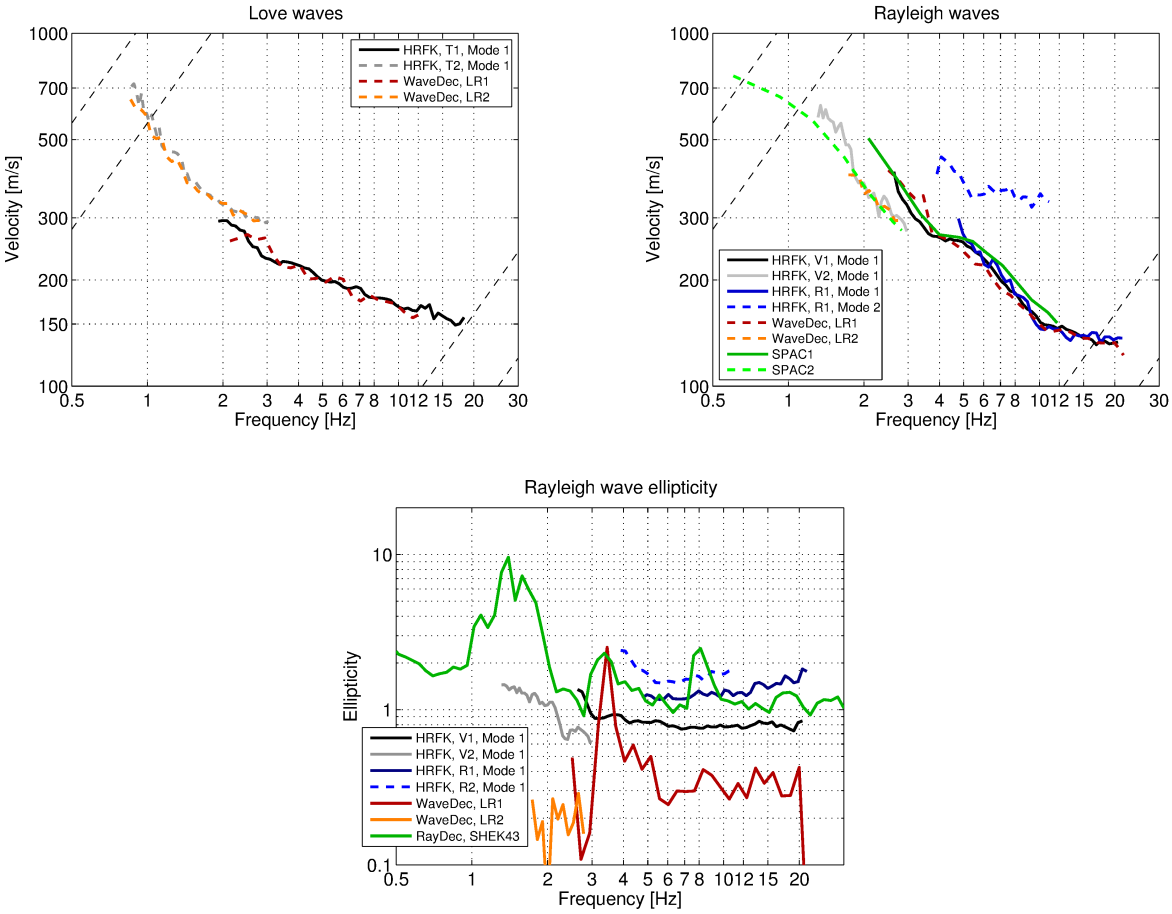

Figure 14: Overview of the Love and Rayleigh wave dispersion curves as well as the ellipticity curves for both arrays. The dashed lines indicate the theoretical resolution limits of the respective arrays (the upper frequency limits corresponds to array 1, the lower one to array 2). The RayDec ellipticity curve corresponds to station SHEK43.

5 Data inversion

5.1 Inversion targets

The targets of the inversion are defined in the following way: the dispersion curves of the small array are deemed to be more reliable because of the smaller spatial heterogeneities of the stations of the arrays (as seen in the H/V curves) and also more representative for station SHEK because of the smaller distances from it. Therefore, the HRFK Love wave dispersion curve from array 1 is completely used as a target and continued to lower frequencies by the low-frequency part of the HRFK Love wave dispersion curve from array 2, but in such a way that both curves can match together. This means that data above 1.7 Hz from array 2 are not used. For the Rayleigh waves, it is not clear how the dispersion curve from array 1 might be continued to lower frequencies with the data from array 2. Therefore, only the HRFK (vertical) dispersion curve from array 1 is used for the Rayleigh waves.
For the ellipticity peak, the RayDec data are used to constrain the left and right flanks and thus constrain the fundamental frequency. The data curves that have been used for the inversion are indicated in Table 2 and are shown in Fig. 15.

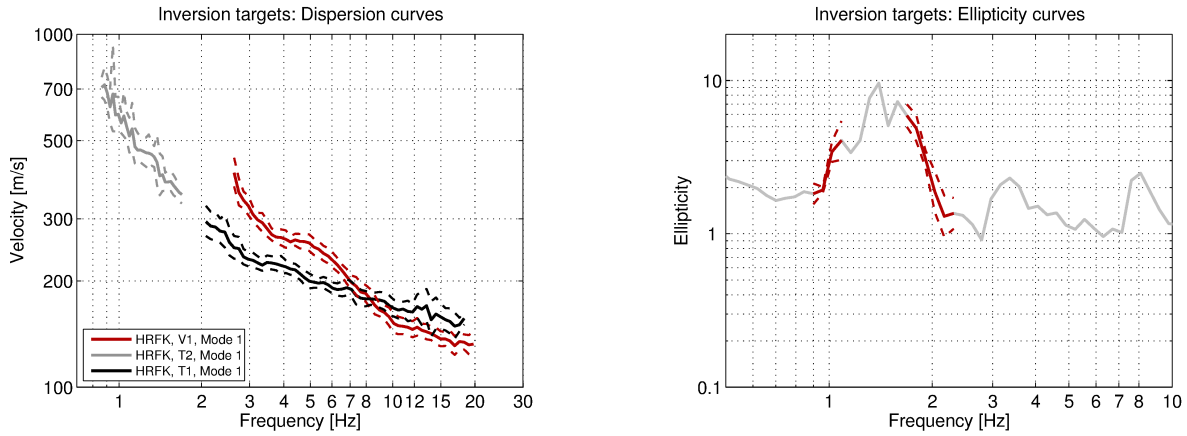

Figure 15: Overview of the dispersion and ellipticity curves used as targets for the different inversions.

Table 2: List of the data curves used as targets in the inversions.

Array	Method	Wave type	Mode	Curve type	Frequency range [Hz]
1	HRFK (V)	Rayleigh	fundamental	dispersion	2.6 - 19.7
2	HRFK (T)	Love	fundamental	dispersion	0.8 - 1.7
1	HRFK (T)	Love	fundamental	dispersion	2.1 - 18.2
1	RayDec (SHEK43)	Rayleigh	fundamental	ellipticity	0.9 - 1.2
1	RayDec (SHEK43)	Rayleigh	fundamental	ellipticity	1.7 - 2.3

5.2 Inversion parameterization

For the inversion, six different parameterizations have been used in total. The first five had free values of the depths and velocities of the different layers, ranging from four to eight layers (including half-space). The last inversion had fixed layer depths and thus consisted of 18 layers in total. In each parameterization, the lowest layers were allowed to range down to 300 m depth. The minimum shear-wave velocity of the top layer was fixed to 50 m/s (v_P to 100 m/s). The density was fixed to 2 300 kg/m^3 for the lowest layer and to 2 000 kg/m^3 for all other layers.

5.3 Inversion results

We performed six inversions with different parameterizations (see Table 3). Each inversion run produced 200 000 total models in order to assure a good convergence of the solution. The results of these inversions are shown in Figs 16 - 21.
All inversions yielded very similar minimum misfit values. This indicated that they all fitted the data equally well, but the best models may still differ. In general, all inversions fit the Rayleigh wave dispersion curve very well and also the ellipticity curve with its peak is well reproduced. For the Love wave dispersion curve, there are minor deviations from the measured curve below 2 Hz.

Table 3: List of inversions

Inversion	Number of layers	Number of models	Minimum misfit
SHEK4layers	4	200 000	0.944
SHEK5layers	5	200 000	0.947
SHEK6layers	6	200 000	0.943
SHEK7layers	7	200 000	0.954
SHEK8layers	8	200 000	0.934
SHEKfixed	18	200 000	0.934

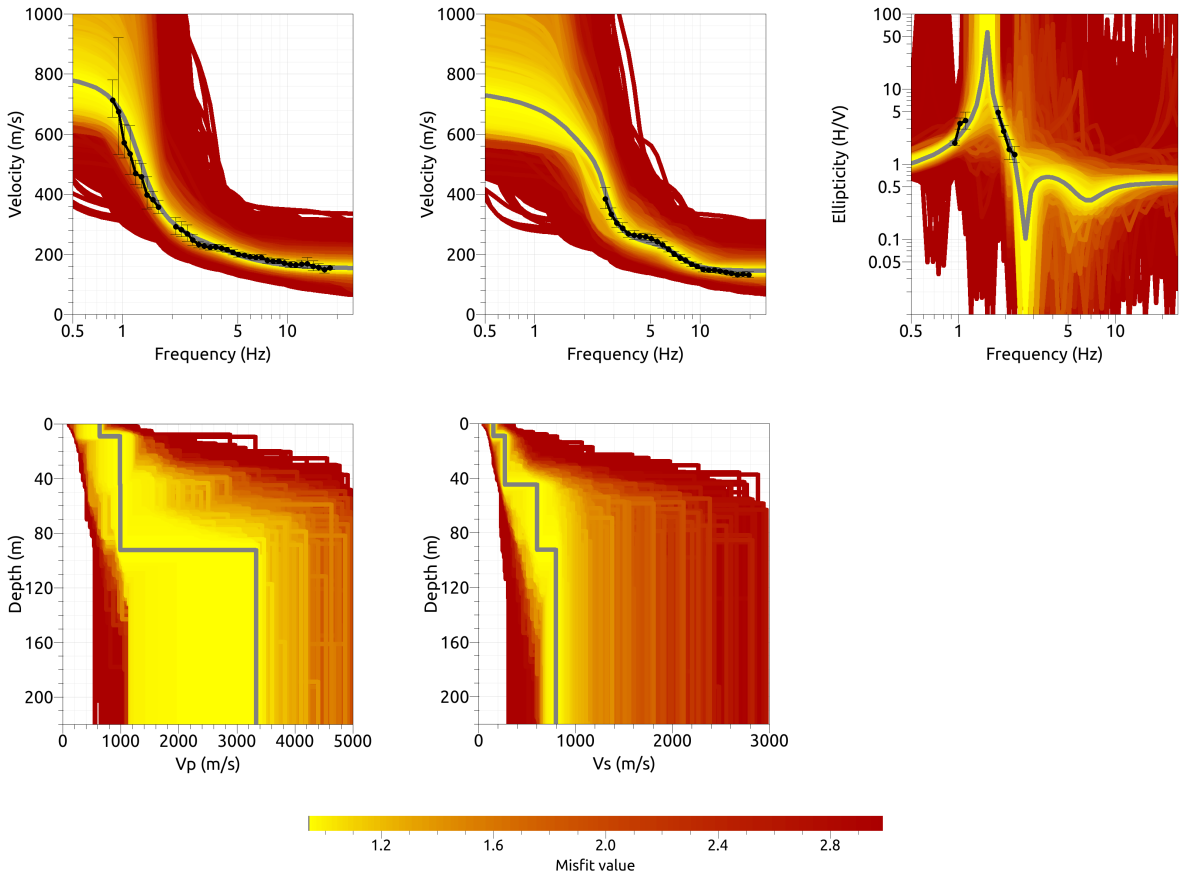

Figure 16: Inversion SHEK4layers: Love wave fundamental mode dispersion curve (top left), Rayleigh wave fundamental mode dispersion curve (top center), Rayleigh wave ellipticity curve (top right), P-wave velocity profiles (center left) and S-wave velocity profiles (center right). The black dots indicate the data points used for the inversion, the gray line indicates the best-fitting model.

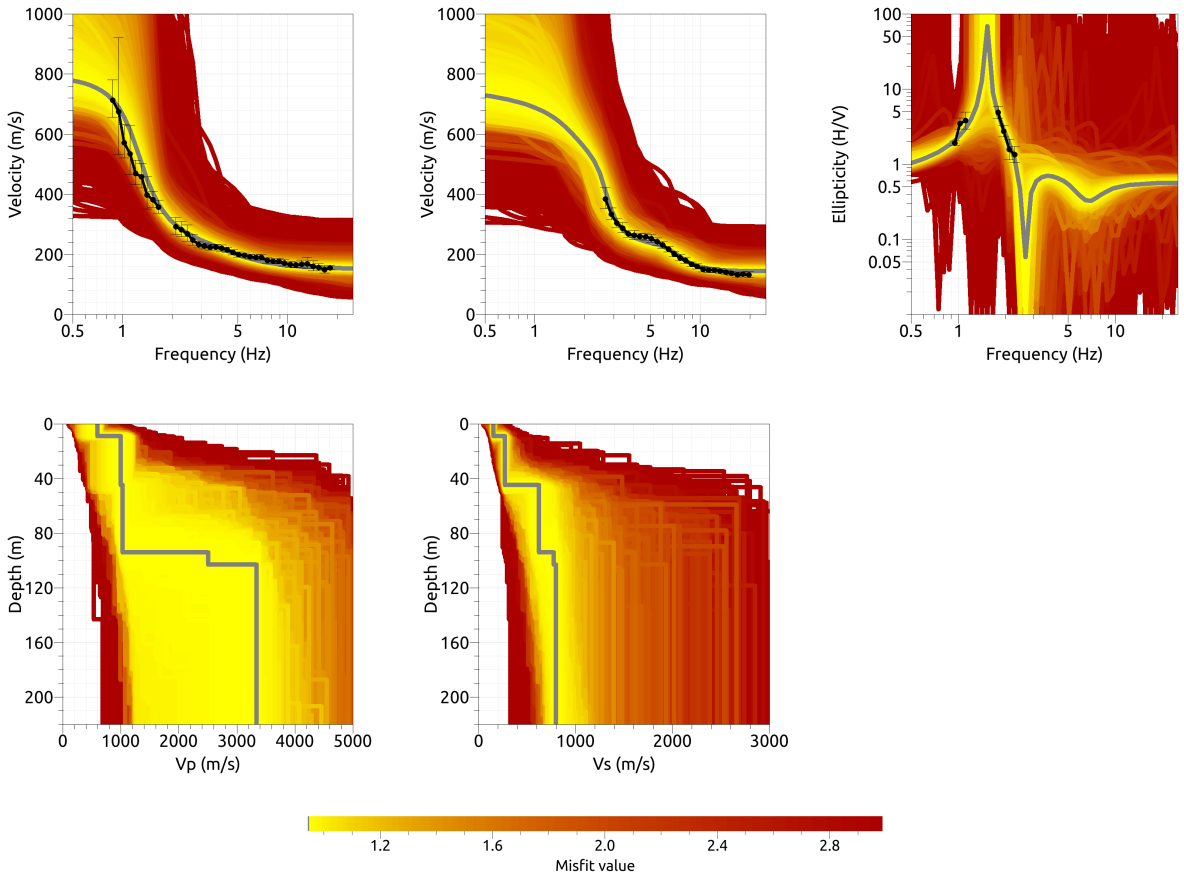

Figure 17: Inversion SHEK5layers: Love wave fundamental mode dispersion curve (top left), Rayleigh wave fundamental mode dispersion curve (top center), Rayleigh wave ellipticity curve (top right), P-wave velocity profiles (center left) and S-wave velocity profiles (center right). The black dots indicate the data points used for the inversion, the gray line indicates the best-fitting model.

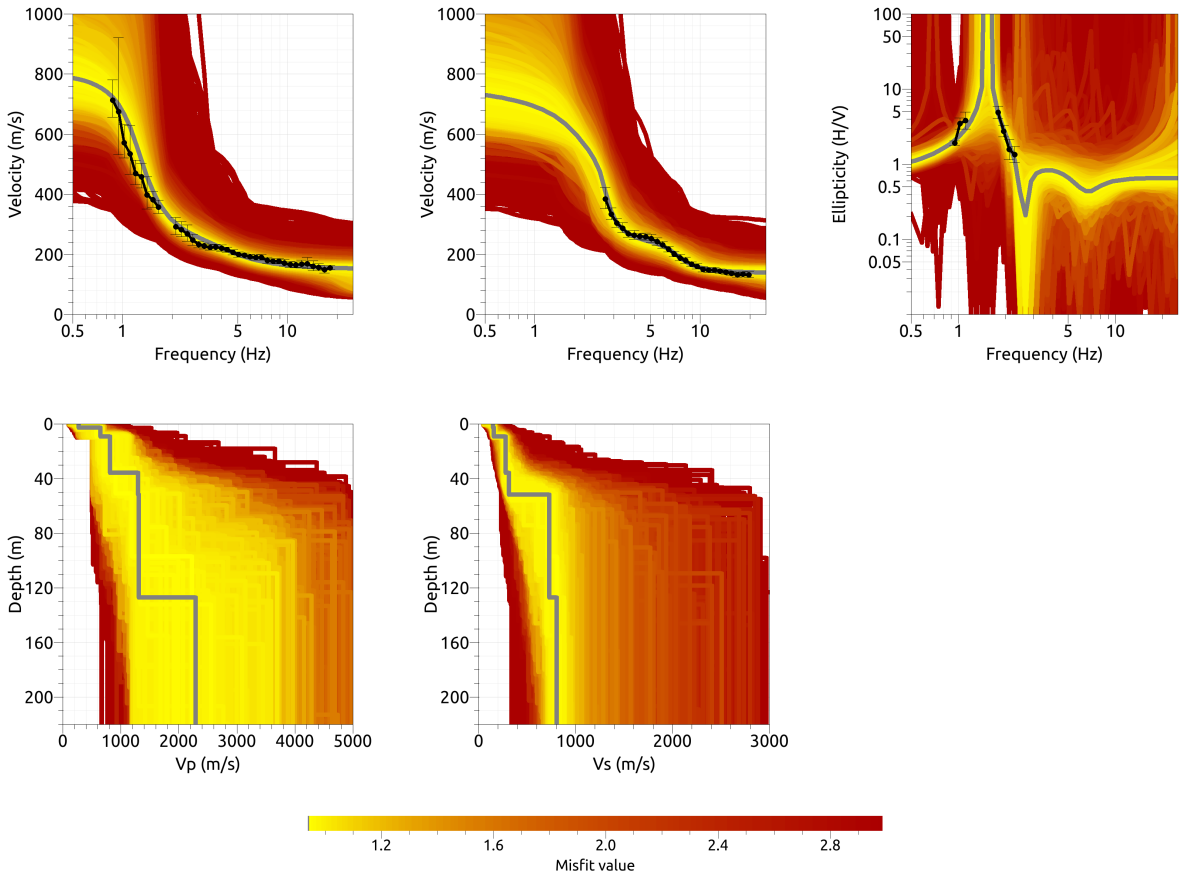

Figure 18: Inversion SHEK6layers: Love wave fundamental mode dispersion curve (top left), Rayleigh wave fundamental mode dispersion curve (top center), Rayleigh wave ellipticity curve (top right), P-wave velocity profiles (center left) and S-wave velocity profiles (center right). The black dots indicate the data points used for the inversion, the gray line indicates the best-fitting model.

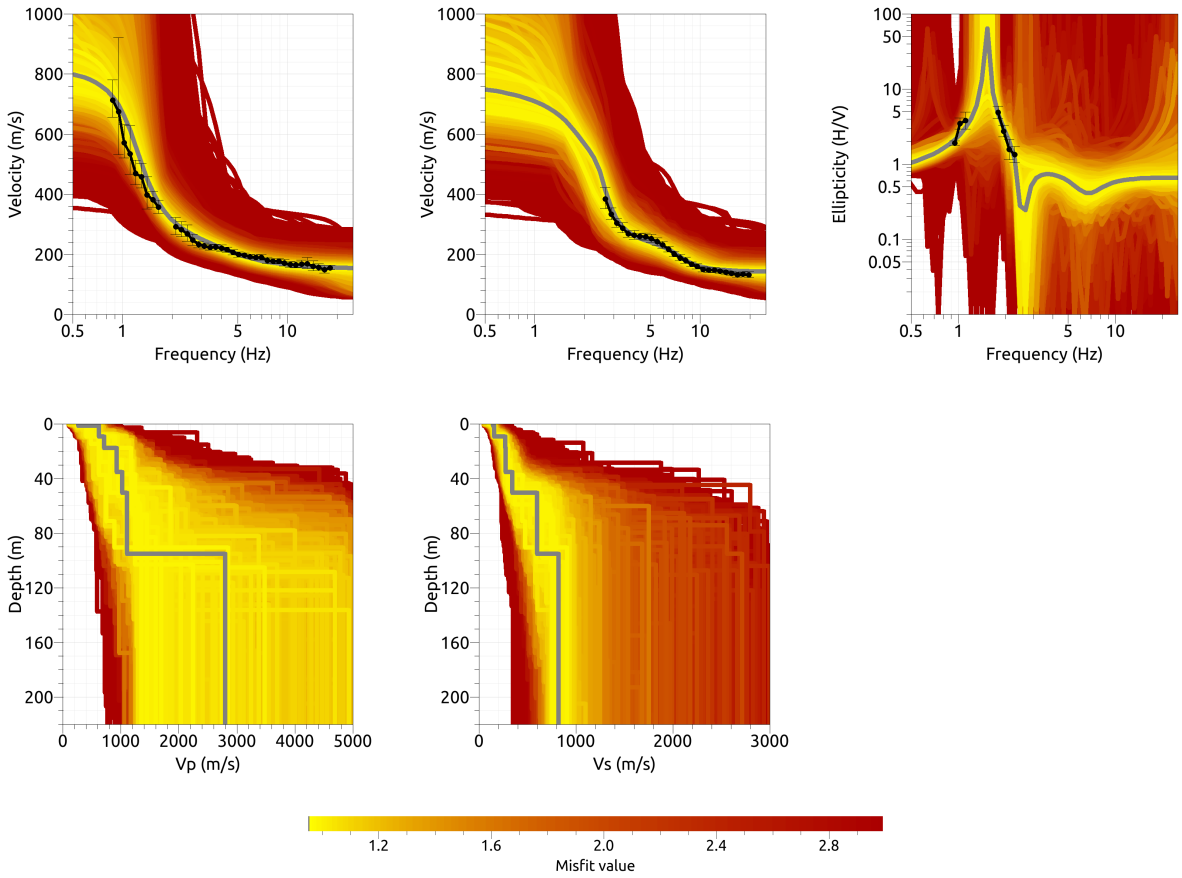

Figure 19: Inversion SHEK7layers: Love wave fundamental mode dispersion curve (top left), Rayleigh wave fundamental mode dispersion curve (top center), Rayleigh wave ellipticity curve (top right), P-wave velocity profiles (center left) and S-wave velocity profiles (center right). The black dots indicate the data points used for the inversion, the gray line indicates the best-fitting model.

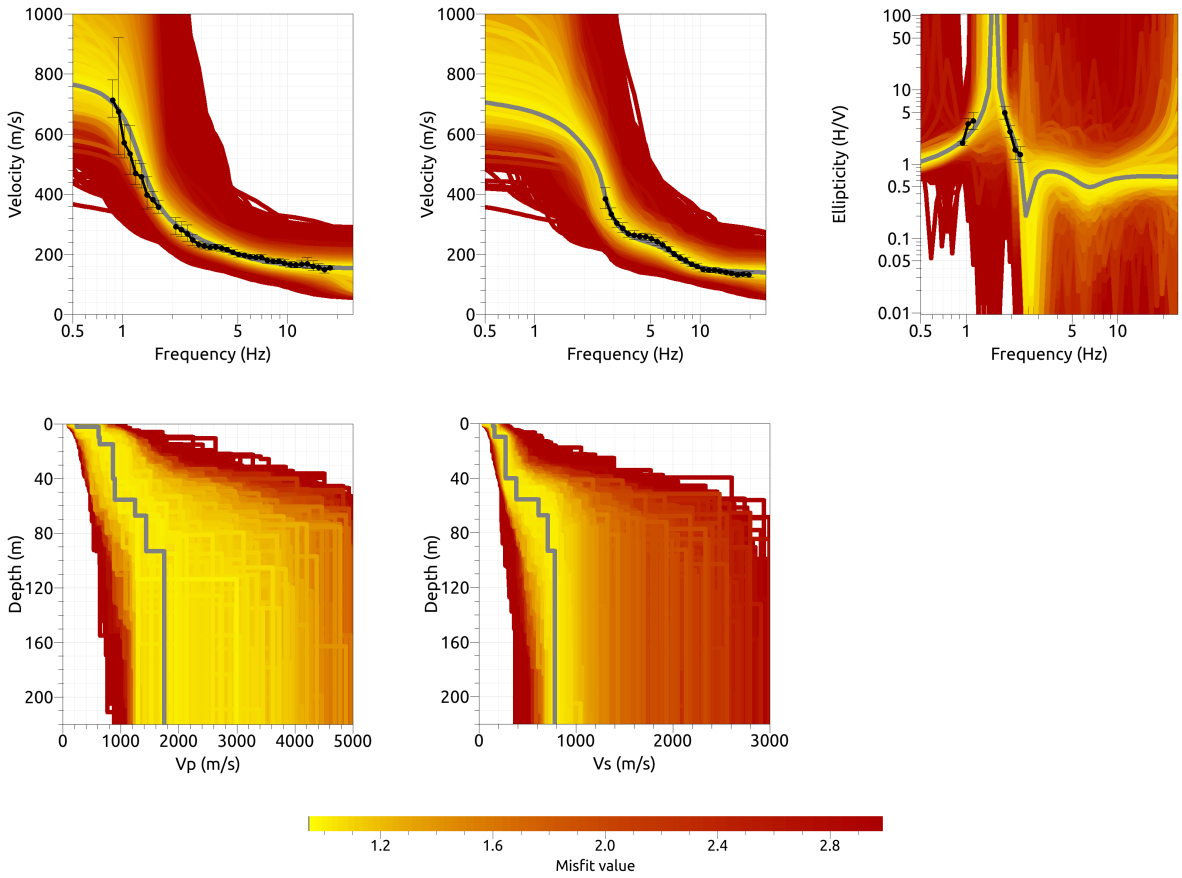

Figure 20: Inversion SHEK8layers: Love wave fundamental mode dispersion curve (top left), Rayleigh wave fundamental mode dispersion curve (top center), Rayleigh wave ellipticity curve (top right), P-wave velocity profiles (center left) and S-wave velocity profiles (center right). The black dots indicate the data points used for the inversion, the gray line indicates the best-fitting model.

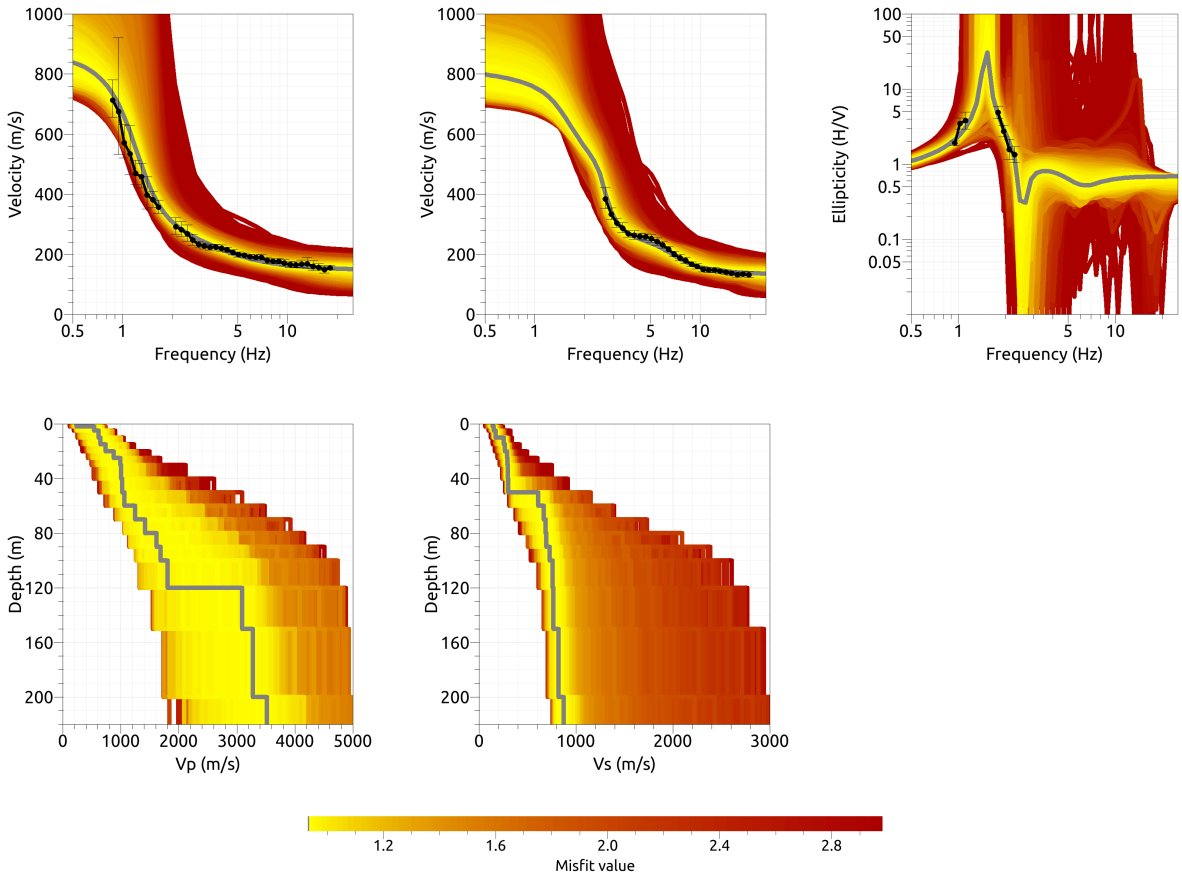

Figure 21: Inversion SHEKfixed: Love wave fundamental mode dispersion curve (top left), Rayleigh wave fundamental mode dispersion curve (top center), Rayleigh wave ellipticity curve (top right), P-wave velocity profiles (center left) and S-wave velocity profiles (center right). The black dots indicate the data points used for the inversion, the gray line indicates the best-fitting model.

5.4 Discussion of the inversion result

The best-fitting models of all inversions are shown in Fig. 22. They all are in very good agreement and show in principle a first layer of about 9 to 10 m thickness with a low shear-wave velocity of about 150 to 160 m/s. The next layer has a velocity of about 270 to 280 m/s down to about 50 m. For some parameterizations, there is another layer with a velocity of about 600 m/s down to about 95 depth. The final layer has a shear-wave velocity of around 800 m/s. The ellipticity peak can be explained by the interface at 50 m depth, so this layer can be characterized as the seismic bedrock. We find this layer deeper than the 30 m that where identified at a borehole nearby.
The average V_{S30} of all inversions is $221 \pm 2\, m/s$, corresponding to soil class C (EC8) or D (SIA261).

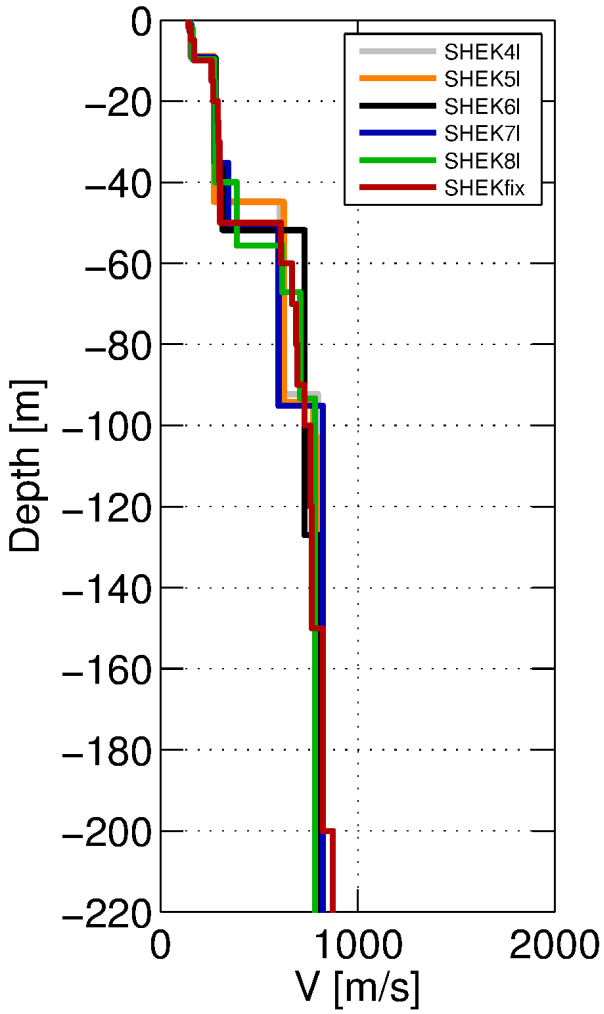

Figure 22: Overview of shear-wave velocity profiles of the best-fitting models of all inversions.

5.5 SH transfer function

The empirical amplification for station SHEK is based on only two events so far so that the statistical quality of the curve will certainly increase in the future. The increasing part of the empirical and the theoretical amplification for the underground models are in good agreement between 0.5 and 1.5 Hz, but the latter shows a peak frequency at 1.5 Hz and the empirical amplification has a rather broad peak around 2 Hz. Between 4 and 6 Hz, the curves coincide again. This could be an indication of edge-generated surface waves (Michel et al., 2014).

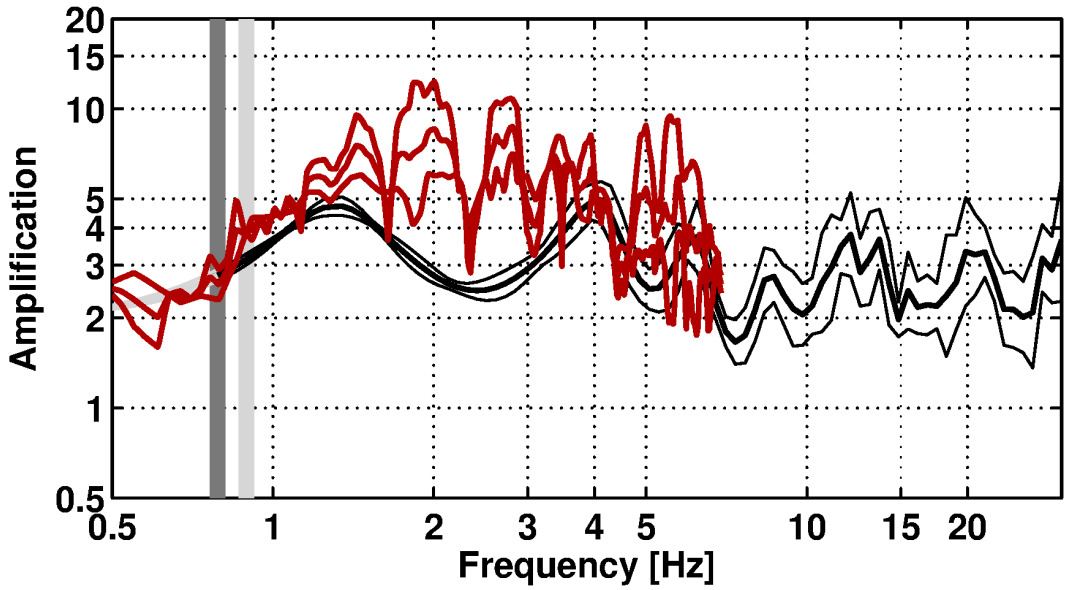

Figure 23: Comparison between the modeled amplification for the best models of the six different inversions (black, with standard deviation) and the empirical amplification measured at station SHEK (red, with standard deviation).

5.6 Quarter-wavelength representation

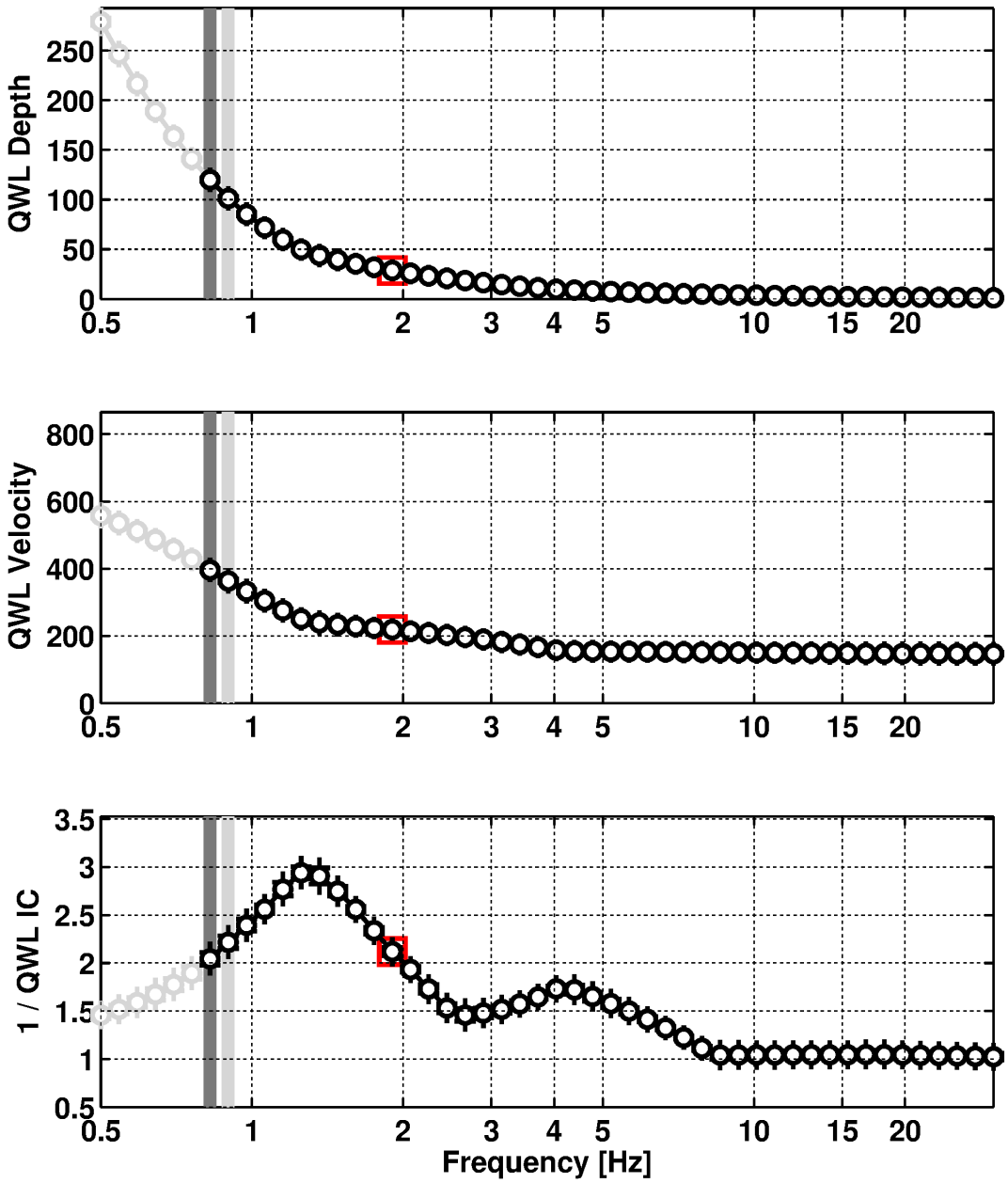

Figure 24: Quarter wavelength representation of the velocity profile for the best models of the six inversions (top: depth, center: velocity, bottom: inverse of the impedance contrast). The black curves are constrained by the dispersion curves, the light grey curves are not constrained by the data. The red square corresponds to V_{S30}.

6 Conclusion

We performed a passive array measurement with two different configurations to characterize the soil underneath station SHEK in Heerbrugg (SG), located close to the basin edge of the Rhine valley.
The dispersion curves for both fundamental Love and Rayleigh waves could be measured well over a wide frequency range, but the results of both array measurements are not perfectly matching, probably due to the higher heterogeneity of the underground structure in the larger array. The ellipticity of the fundamental Rayleigh wave mode was also measured with several techniques and shows a clear peak at 1.6 Hz.
The joint inversion of Love and Rayleigh wave dispersion and ellipticity curves showed that the structure can be well explained by at least four layers. All inversions show a superficial layer of around 9 m thickness with an S-wave velocity of about 150 m/s, followed by a second layer of about 270 m/s down to about 50 m. Some inversions show indications for another interface at around 95 m depth, but the interface at 50 m can be characterized as the seismic bedrock. The V_{S30} of the best models is about 220 m/s, corresponding to soil class C in EC8 and D in SIA261.

Acknowledgements

The authors thank David Farsky and André Robert for their help during the array measurements.

References

Aki, K. (1957). Space and time spectra of stationary stochastic waves, with special reference to microtremors. *Bull. Earthquake Res. Inst. Tokyo Univ.*, 35:415–456.

Bettig, B., Bard, P.-Y., Scherbaum, F., Riepl, J., Cotton, F., Cornou, C., and Hatzfeld, D. (2001). Analysis of dense array noise measurements using the modified spatial auto-correlation method (SPAC): application to the Grenoble area. *Boll. Geof. Teor. Appl.*, 42:281–304.

Burjánek, J., Gassner-Stamm, G., Poggi, V., Moore, J. R., and Fäh, D. (2010). Ambient vibration analysis of an unstable mountain slope. *Geophys. J. Int.*, 180:820–828.

Burjánek, J., Moore, J. R., Molina, F. X. Y., and Fäh, D. (2012). Instrumental evidence of normal mode rock slope vibration. *Geophys. J. Int.*, 188:559–569.

Fäh, D., Wathelet, M., Kristekova, M., Havenith, H., Endrun, B., Stamm, G., Poggi, V., Burjanek, J., and Cornou, C. (2009). Using ellipticity information for site characterisation. NERIES deliverable JRA4 D4, available at http://www.neries-eu.org.

Hobiger, M., Bard, P.-Y., Cornou, C., and Le Bihan, N. (2009). Single station determination of Rayleigh wave ellipticity by using the random decrement technique (RayDec). *Geophys. Res. Lett.*, 36.

Maranò, S., Reller, C., Loeliger, H.-A., and Fäh, D. (2012). Seismic waves estimation and wavefield decomposition: Application to ambient vibrations. *Geophys. J. Int.*, 191:175–188.

Michel, C., Edwards, B., Poggi, V., Burjánek, J., Roten, D., Cauzzi, C., and Fäh, D. (2014). Assessment of site effects in alpine regions through systematic site characterization of seismic stations. *Bull. Seismol. Soc. Am.*, 104:–.

Poggi, V. and Fäh, D. (2010). Estimating Rayleigh wave particle motion from three-component array analysis of ambient vibrations. *Geophys. J. Int.*, 180:251–267.